RIS Aided B5G V2V Solution for Road Safety Applications

Tathagat Pal
2019211

BTP report submitted in partial fulfillment of the requirements
for the Degree of B.Tech. in Electronics and Communication & Engineering
on 25/12/2022

BTP Track: Research Project

BTP Advisors
Dr. Vivek Ashok Bohara
Prof. Anand Srivastava

Indraprastha Institute of Information Technology
New Delhi

Student's Declaration

I hereby declare that the work presented in the report entitled **Optical RIS Aided B5G V2V Solution for Road Safety Applications** submitted by me for the partial fulfillment of the requirements for the degree of *Bachelor of Technology* in *Electronics and Communication & Engineering* at Indraprastha Institute of Information Technology, Delhi, is an authentic record of my work carried out under guidance of **Dr. Vivek Ashok Bohara and Prof. Anand Srivastava**. Due acknowledgements have been given in the report to all material used. This work has not been submitted anywhere else for the reward of any other degree.

Tathagat Pal **Date: 25/12/2022**
Student's Name

Certificate

This is to certify that the above statement made by the candidate is correct to the best of my knowledge.

Dr. Vivek Ashok Bohara & Prof. Anand Srivastava **Date: 25/12/2022**
Advisors' Name(s)

Abstract

Terahertz (THz) communication is a viable technology for the 6G wireless networks. THz frequencies often have a limited coverage area because of their extremely high spread attenuation and molecular absorption. Consequently, new methods are necessary to get around these limitations. Additionally, reconfigurable intelligent surfaces (RIS) are used to modify the wireless propagation environment and enhance the coverage area. As a result, we highlight the benefit of deploying RIS for enhanced vehicular message dissemination. We utilize a novel moment-generating functional based approach to derive the ergodic signal-to-noise ratio (SNR) for the proposed system. Numerical results and findings reveal that the proposed RIS aided THz-V2V system can significantly enhance BER and sumrate performance as compared to opical IRS aided vehicular-visible light communication (V-VLC). Moreover, the project demonstrates the impact of different weather conditions such as snow, rain, etc. on the proposed RIS-aided THz-V2V communication system in terms of SNR and BER.

Contents

Chapter 1

Introduction

Terahertz (THz) waves are electromagnetic waves that lie within the electromagnetic spectrum's range of 0.1 to 10 THz. It is an uninvestigated band gap that is open to fresh study objectives. THz technology, essentially bridges the gap between radio and optical frequency ranges, has promise for next-generation wireless networks. Beyond 5G, which enables a large number of connected devices and significantly greater user data rates, the THz band is regarded as one of the main sources of pervasive wireless communications. THz waves enable stronger link directivity, higher user densities, improved dependability, and less delay due to their shorter wavelength [1]. Traffic congestion and accidents are two common issues in the transportation industry. Because of this, communication between vehicles has become more crucial recently in an endeavor to enhance road safety [2]. Technologies such as vehicle-to-vehicle (V2V), infrastructure-to-vehicle (I2V), vehicle-to-infrastructure (V2I) and vehicle-to-everything (V2X) are aimed at providing communication techniques that vehicles potentially utilise in diverse application scenarios [3]. However, because of the extremely high frequency and the resulting significant signal attenuation due to path loss propagation, THz is only viable in short-range communication settings [4, 5]. Additionally, spreading loss increases with frequency, leading to substantial path loss from molecular absorption spurred on by water vapour and oxygen molecules. As a result, communication is interrupted because line-of-sight (LoS) obstructions can easily block THz routes due to significant absorption.

A cutting-edge technology called reconfigurable intelligent surfaces (RIS) has the potential to effectively increase wireless network coverage. Each of the separate passive reflecting surfaces of a RIS can change the configuration of incident THz signal by modifying the signal's phase [6]. As a result, it reduces THz's vulnerability to obstruction and expands the coverage area for outdoor applications [7]. Wireless network's spectral efficiency is increased and multiple LoS links are created between the communication points due to RIS. As a result, RIS's capabilities entices more for THz frequency spectrum. Of this and other benefits of RIS drive us to investigate an effective RIS-assisted THz-V2V communication system for next generation systems.

Chapter 2

Motivation and Research Problem

Figure 2.1: Real life application scenario: At road intersection, the vehicles in blocked LOS (dashed red line) can communicate via RIS (green line) for better system performance.

THz band analysis reveals that these frequencies have a plethora of advantages over optical frequencies. THz waves are seen as potential uplink communication carriers. They enable non-line-of-sight (NLoS) propagation [8] and serve as suitable replacements in adverse weather situations such fog, dust, and turbulence [9]. The THz frequency spectrum is also unaffected by ambient noise from optical sources and is not constrained by any safety or health requirements [10].

Motivated by the above insights, this research project directs to highlight the benefits of RIS aided THz based V2V communication over O-IRS aided V-VLC [11] for enhanced vehicular message dissemination particularly at road crossing. Further, we also provide a comparative study on the impact of adverse weather conditions such as rain and snow on the performance of RIS aided THz as well as O-IRS aided VLC based V2V communication [12].

Fig. 3.1 depicts the system model of the suggested RIS aided THz-V2V system. The distances d_{SR} and d_{RD} stand for the separations between the source vehicle, V_S and RIS and destination vehicle, V_D, respectively. The single antenna V_S and single antenna V_D are connected through RIS. Given the significant propagation loss at the THz frequency, direct communication between the $V_S - V_D$ is precluded [13]. The high THz frequencies cause reflection and scattering of the signal which has minimal roles in the received signal power. As a result, LoS path is taken into account in the V_S-RIS and RIS$-V_D$ linkages. Additionally, we assume that both the V_S and the V_D have access to the channel state information (CSI).

Chapter 3

System Model

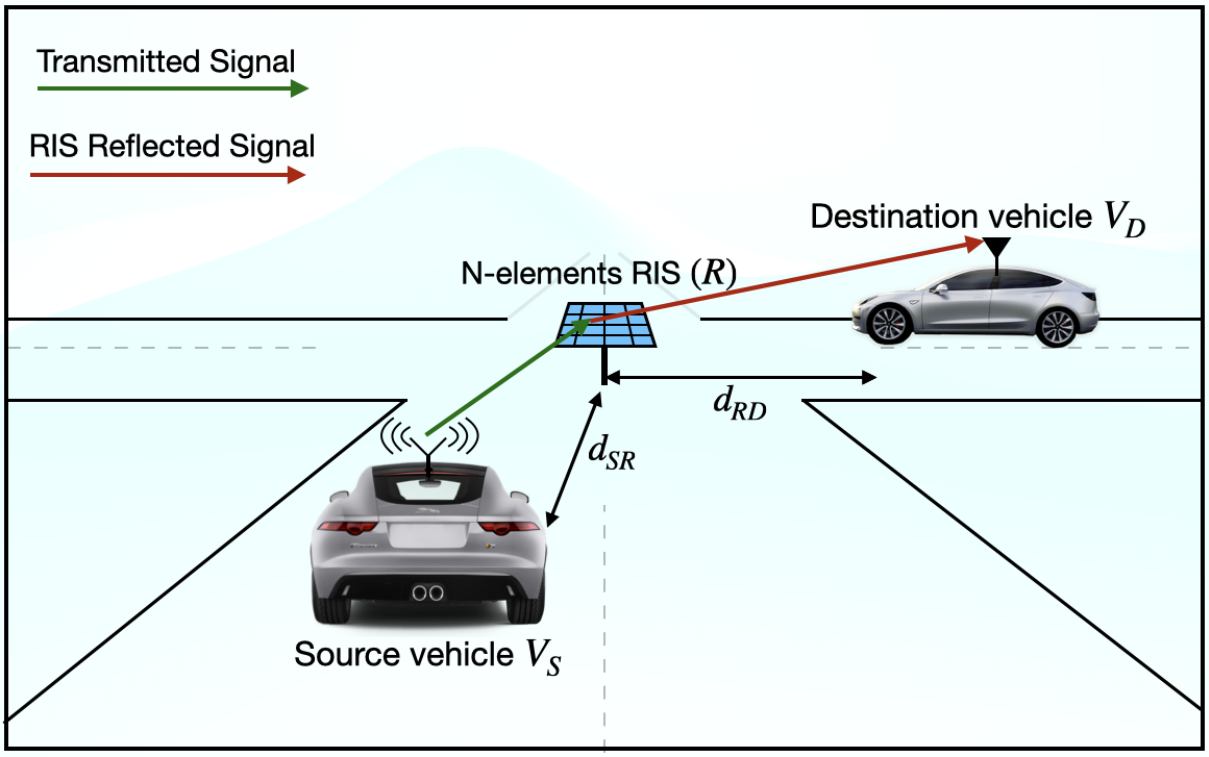

Figure 3.1: RIS deployed at road intersection to facilitate THz based V2V communication.

3.1 RIS-aided THz-V2V Channel Modelling

Since the strength of the scattering component in THz transmission is typically substantially lower (more than 20 dB) than the power of the LoS component [13], we disregard the scattering component. The channel between the source vehicle S and the destination vehicle V_D should

therefore be dominated by the RIS modified link, given as:

$$H(f,d) = \sum_{i=1}^{N} \mathbf{H}^{i}_{RIS}(f, d_{SR}, d_{RD}), \tag{3.1}$$

where $\mathbf{H}^{i}_{RIS}(f, d_{SR}, d_{RD})$ are V_S-RIS-V_D channels. The carrier frequency is denoted by f, whereas d_{SR}, d_{RD} represent the distances between V_S-RIS and RIS$-V_D$, respectively.

$$\sum_{i=1}^{N} H^{i}_{RIS}(f, d_{SR}, d_{RD}) = \sum_{i=1}^{N} \zeta_{PL} G^{i}_{SR}(f, d_{SR}) e^{j\phi_i} G^{i}_{RD}(f, d_{RD}), \tag{3.2}$$

where ϕ_i is the adjustable phase induced by i^{th} reflecting element of the RIS, $G^{i}_{SR}(f, d_{SR}) = l_{THz}(f, d_{SR})\alpha_i e^{-j\theta_i}$ is the V_S-RIS^i channel gain, $G^{i}_{RD}(f, d_{RD}) = l_{THz}(f, d_{RD})\beta_i e^{-j\psi_i}$ is the RIS^i-V_D channel gain. $\zeta_{PL} = \frac{2\sqrt{2\pi}d^2_{IRS}}{\lambda^2}$ is the the path-loss compensation factor. Further, l_{THz} represents the path loss consisting of the free-spread loss and the molecular absorption loss in THz communication and satisfies $l_{THz}(f, d) = \frac{c}{4\pi f d} e^{-\frac{1}{2}\tau(f)d}$.

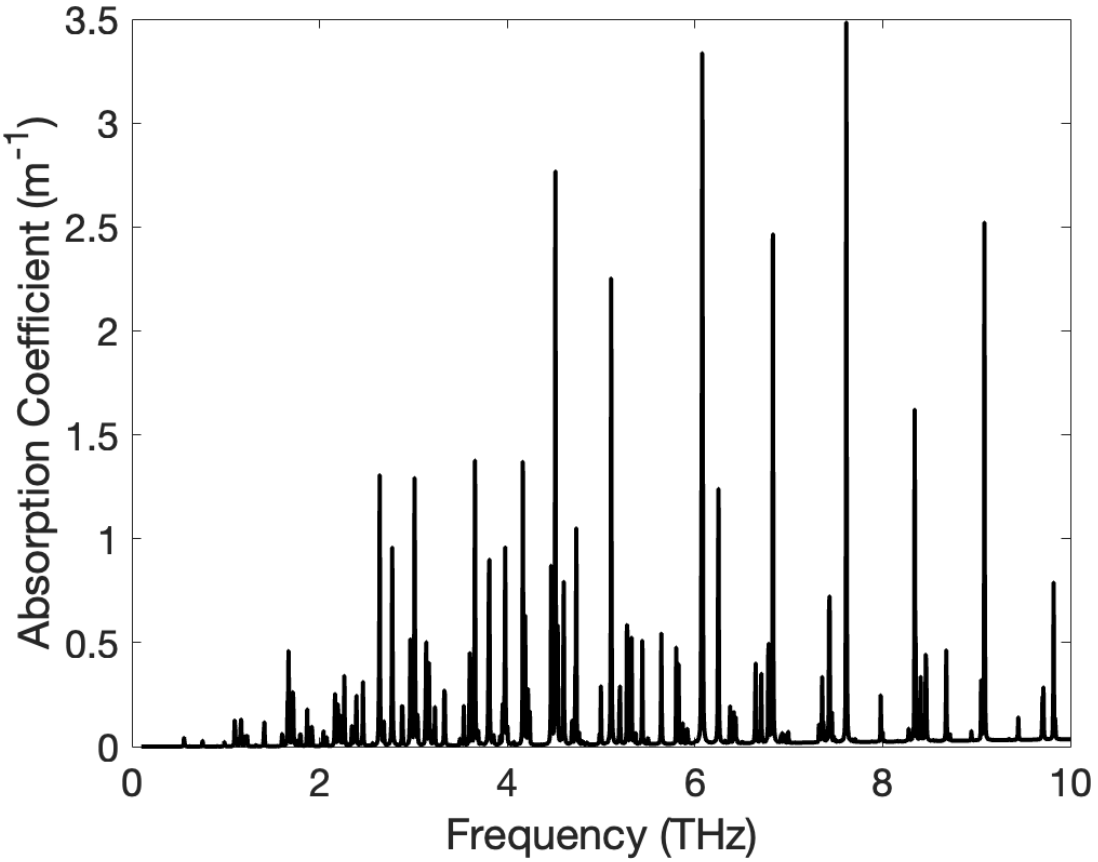

Figure 3.2: Molecular absorption loss, $\tau(f)$ in m^{-1} for water vapour varying with frequency..

However, water vapour molecules make up the majority of the overall absorption in a regular medium (Fig. 3.2), with more than 4,000 resonant peaks throughout the entire band and

absorption coefficients six orders of magnitude higher than those of the oxygen resonances [14]. The water vapour molecules present in a typical medium already have a major impact on the channel performance in the Terahertz Band, as opposed to the attenuation brought on by fog or raindrops in traditional RF systems in the megahertz and gigahertz spectrum.

In matrix form, we can re-write (3.2) as:

$$\sum_{i=1}^{N} H_{RIS}^{i}(f, d_{SR}, d_{RD}) = \zeta_{PL}\mathbf{G}_{RD}(f, d_{RD})^{T}\mathbf{\Phi}\mathbf{G}_{SR}(f, d_{SR}), \tag{3.3}$$

where $\mathbf{G}_{SR}(f, d_{SR}) = \begin{bmatrix} G_{SR}^{1} & G_{SR}^{2} & \cdots & G_{SR}^{N} \end{bmatrix}^{T}$ and $\mathbf{G}_{RD}(f, d_{RD}) = \begin{bmatrix} G_{RD}^{1} & G_{RD}^{2} & \cdots & G_{RD}^{N} \end{bmatrix}^{T}$. The channel links $\mathbf{G}_{SR}(\in C^{1\times N})$ and $\mathbf{G}_{RD}(\in C^{N\times 1})$ follow a Rician distribution as follows:

$$\mathbf{G}_{SR} = \left(\sqrt{\frac{k}{k+1}}G_{SR}^{LoS} + \sqrt{\frac{1}{1+k}}G_{SR}^{NLoS}\right), \tag{3.4}$$

and

$$\mathbf{G}_{RD} = \left(\sqrt{\frac{k}{k+1}}G_{RD}^{LoS} + \sqrt{\frac{1}{1+k}}G_{RD}^{NLoS}\right), \tag{3.5}$$

3.2 SNR Calculation

The signal-to-noise ratio (SNR), γ at the destination vehicle, V_D is given as:

$$\gamma = \frac{|\sum_{i=1}^{N}\zeta_{PL}l_{THz}^{SR}\alpha_i l_{THz}^{RD}\beta_i e^{j(\phi_i-\theta_i-\psi_i)}|^2 E_s}{N_0}, \tag{3.6}$$

where E_s is the average transmitted energy per symbol. It is easy to deduce that γ is maximized by removing the channel phases (similar to co-phasing in traditional maximum ratio combining schemes), meaning that the best option of ϕ_i for maximising the γ is $\phi_i = \theta_i + \psi_i$ for $i = 1, \cdots, N$. Notably, this method necessitates that the RIS is aware of the channel phases. The sequel discusses how to perform channel estimation in RIS-enabled wireless systems. Additionally, the ideal selection of the phases, $\phi_i = \theta_i + \psi_i$, $i = 1, \cdots, N$ is obtained from the identity:

$$\Big|\sum_{i=1}^{N} z_i e^{j\omega_i}\Big|^2 = \sum_{i=1}^{N} z_i^2 + 2\sum_{i=1}^{N}\sum_{k=i+1}^{N} z_i z_k \cos(\omega_i - \omega - k), \tag{3.7}$$

which is maximized if $\omega_i = \omega$, for all i.

Using (3.6) and (3.7), SNR could be maximized as follows [15]:

$$\gamma_{max} = \frac{|\Upsilon\sum_{i=1}^{N}\alpha_i\beta_i|^2 E_s}{N_0} \tag{3.8}$$

where $\Upsilon = \zeta_{PL} l_{THz}^{SR} l_{THz}^{RD}$. For large N, i.e., $N >> 1$, $\gamma_{max} \approx \frac{\Lambda^2 E_s}{N_0}$, where $\Lambda = \Upsilon \sum_{i=1}^{N} \alpha_i \beta_i$. Since α_i and β_i are independently distributed Rician RVs, the mean value and the variance of their product are $E[\alpha_i \beta_i] = \frac{\pi}{4} L_{\frac{1}{2}}^2(-k)$ and $VAR[\alpha_i \beta_i] = 1 - \frac{\pi^2}{16(1+k^2)} L_{\frac{1}{2}}^4(-k)$, where $L_{\frac{1}{2}}(\cdot)$ is Laguerre polynomial of degree $\frac{1}{2}$. The central limit theorem states that for a sufficient number of reflecting meta-surfaces elements, Λ converges to a Gaussian distributed random variable with mean:

$$E[\Lambda] = N\Upsilon \frac{\pi}{4} L_{\frac{1}{2}}^2(-k), \tag{3.9}$$

and variance:

$$VAR[\Lambda] = N\Upsilon^2 \left(1 - \frac{\pi^2}{16(1+k^2)} L_{\frac{1}{2}}^4(-k)\right). \tag{3.10}$$

where $L_{\frac{1}{2}}(\cdot)$ is degree-$\frac{1}{2}$ Laguerre polynomial. Consequently, moment generating function (MGF) of γ_{max} is given by considering it a non-central chi-square random variable with one degree of freedom. The MGF, $M_{\gamma_M}(\tau)$ is written as follows [16]:

$$\begin{aligned} M_{\gamma_M}(\tau) = & \sqrt{\frac{1}{1 - 2\tau N \Upsilon^2 \left(1 - \frac{\pi^2}{16(1+k^2)} L_{\frac{1}{2}}^4(-k)\right) \frac{E_s}{N_0}}} \\ & \times \exp\left(\frac{\frac{\tau N^2 \Upsilon^2 \pi^2 E_s}{16 N_0}}{1 - 2\tau N \Upsilon^2 \left(1 - \frac{\pi^2}{16(1+k^2)} L_{\frac{1}{2}}^4(-k)\right) \frac{E_s}{N_0}}\right) \end{aligned} \tag{3.11}$$

The average received SNR can be expressed as follows:

$$E[\gamma] = \frac{N^2 \pi^2 \psi + \Upsilon^2 N (16(1+k^2) - \pi^2 L_{\frac{1}{2}}^4(-k)) E_s}{16(1_k^2) N_0}, \tag{3.12}$$

where $\psi = \Upsilon^2 L_{\frac{1}{2}}^4(-k)(1+k^2)$.

3.3 Symbol Error Probability

Using (3.11), the M-ary phase shift keying (PSK) signaling's average SEP can be calculated as [17]:

$$P_e = \frac{1}{\pi} \int_0^{\frac{(M-1)\pi}{M}} M_\gamma \left(\frac{-\sin^2(\frac{\pi}{M})}{\sin^2 \xi}\right) d\xi. \tag{3.13}$$

Additionally, the system's sumrate Γ (bps/Hz) is stated as:

$$\Gamma = \log_2(1 + \gamma_{max}). \tag{3.14}$$

Consequently, the sumrate of RIS-assisted THz-V2V communication system depends on N,

which is further demonstrated in the results and discussion section.

3.4 Effect of Snow and Rain on THz-V2V Communication Facilitated by RIS

THz wireless outdoor communication applications necessitate research on link performance under a variety of atmospheric conditions, such as snow, rain, fog, clouds, and haze. Here, we give theoretical analyses of THz wave propagation through layers of snow and during snowfall.

Mie theory is typically used to investigate how the snow particles scatter the THz radiation. This makes sense because snowflakes often range in size from order of 10^{-3}m to $10^{-2}m$ [18], which equals or surpasses the THz range requirements.

The absorption and scattering coefficients can be used to explain the scattering properties of a transmitted THz signal. Initially, it is necessary to presumptively disregard multiple scattering, and then, it assume that each scatter responds regardless from the rest. Based on these generalizations, a THz signal travelling over snow experiences an attenuation of [19]:

$$\mathcal{A} = 4.343 \times 10^3 \int_0^\infty \sigma_{ext}(m, r, \lambda) N(r) dr, \tag{3.15}$$

where $N(r)$ is the snow size distribution and m is the particle's refractive index. The extinction cross-section, $\sigma_{ext}(m, r, \lambda) = \sigma_{abs}(m, r, \lambda) + \sigma_{sca}(m, r, \lambda)$, represents the total absorption cross-section $\sigma_{abs}(m, r, \lambda)$ and the scattering cross-section $\sigma_{sca}(m, r, \lambda)$.

Adding on to that, $N(r) = N_0 \exp(-\varpi r)$, where N_0 is the count of snowflakes. The radius of each snow particle is $r + dr$ per unit volume in m^{-3} mm^{-1}. The molten snow particles' radius is depicted by r, and R represents equivalent rate of rainfall in mm hr^{-1}; ϖ is a distinctive characteristic that can be recovered by snowfall rate. According to Gunn-Marshall distribution, $N_0 = 7.6 \times 10^3 R^{0.87}$ and $\varpi = 5.1 R^{-0.48}$. The G-M snow size distribution is utilised here. Similarly, for characterizing rain-drop distribution, we utilize Marshall-Palmer distribution, according to which, $N_0 = 16 \times 10^3$ and $\varpi = 8.2 R^{-0.21}$.

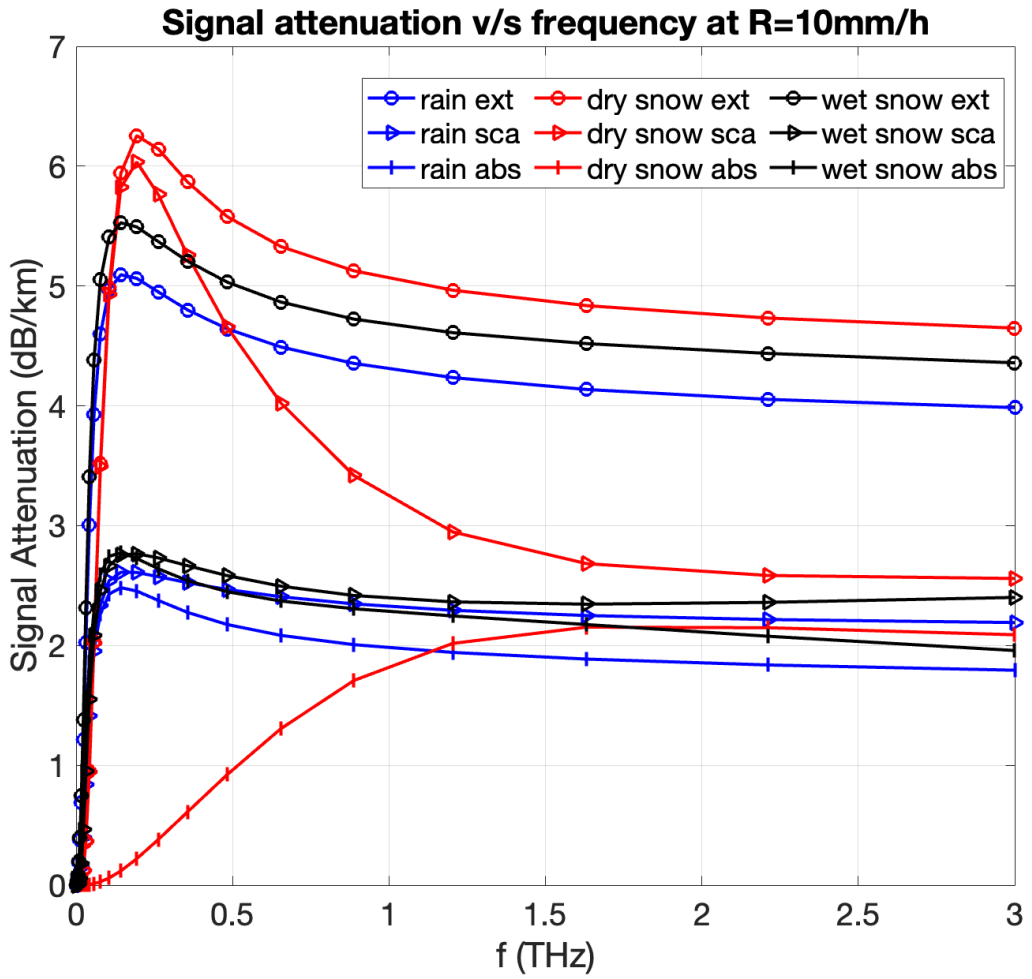

Figure 3.3: Attenuation loss $\mathcal{A}$ as a function of frequency for dry snow, wet snow (25% water content) and rain, $R = 10$mm/hr.

Evident from Fig.3.3, as a result of the low water content, we can see that the extinction attenuation in dry snow is primarily caused by the scattering effect. However, in wet snow, high water content absorption exerts an effect that is comparable to that of scattering. Moreover, wet snow contains a significant amount of water, therefore the attenuation ought to be similar to that caused by rain. At lower frequencies, dry snow with a substantially less water in it should result in significantly lower attenuation than rainfall with a comparable fall rate. On the contrary, at higher frequencies, that is, for frequencies more than 200 GHz (0.2 THz) more attenuation due to dry snow than due to rain could be observed.

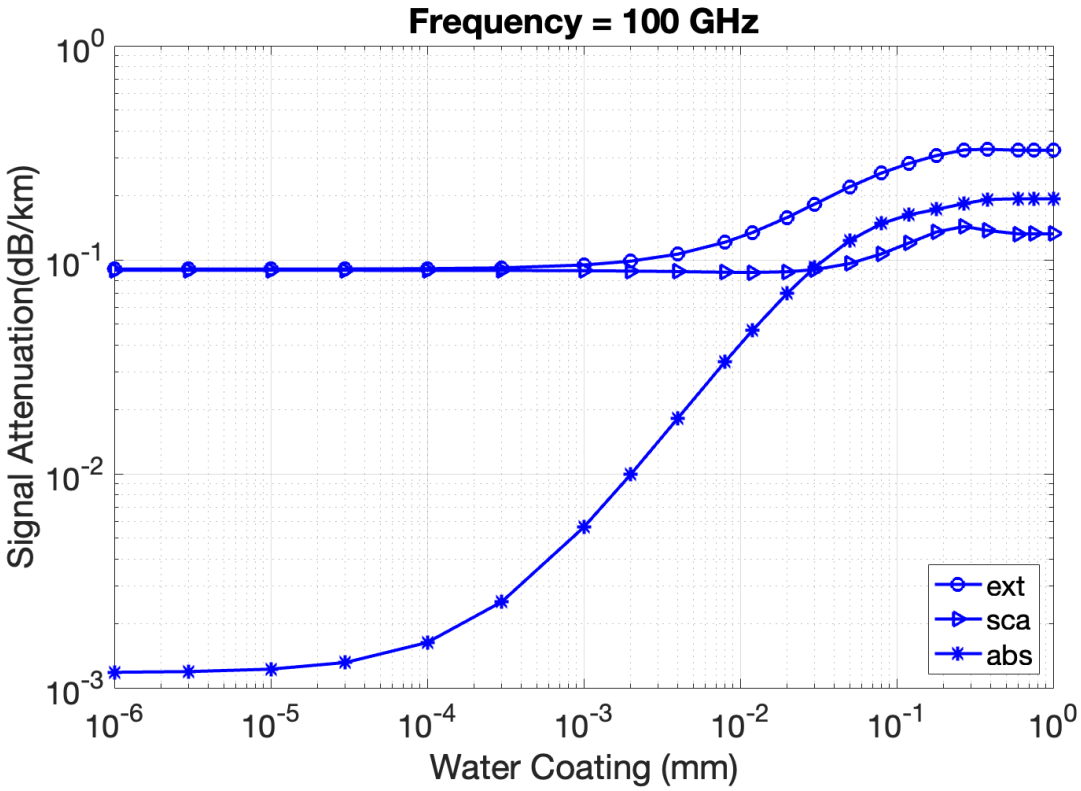

Figure 3.4: Impact of water-coating thickness (mm) on signal attenuation $\mathcal{A}$, at a frequency of 100 GHz.

We also present the impact of water coating on the signal attenuation $\mathcal{A}$ in Fig. 3.4. It could be observed from the plot that increasing thickness from 10^{-6} to 10^{-3}mm has a negligible effect on the extinction and scattering attenuation. Whereas, since the thickness of the water coating increases, it acts more like a rain drop and consequently, the absorption component starts predominating the scattering one.

Chapter 4

Results and Discussions

The utility of RIS in THz-V2V communication is demonstrated in this section using the results of simulations. We take into account the transmitted power of 1 watt and the noise PSD N_0 of 10, 90 dBm/GHz. We also analyze the impact of weather conditions like snow and rain on the proposed system. Until specifically mentioned, we consider carrier signal frequency, f to be 400 GHz and distance from RIS to V_D, d_{RD} to be 10 m. Further, we use BPSK ($M = 2$ in (**??**)) modulation scheme.
Also, $d_{SR} = d_1$ and $d_{RD} = d_2$ could be used interchangeably.

We present the following results:
1. SNR v/s Frequency for different N, d_{SR} and atmospheric conditions [RIS aided THz-V2V]

2. SNR v/s d_{SR} for different N, varying K and compare the results for RIS aided THz-V2V v/s O-IRS aided V-VLC.

3. Sumrate v/s d_{SR} and P_T for $N = 64, 256$.

4. BER v/s N for RIS aided THz-V2V v/s O-IRS aided V-VLC for different $d_1 = d_2$.

5. BER v/s P_T for THz-V2V under various atmospheric conditions.

4.1 SNR v/s Frequency: THz-V2V under Normal Weather Condition v/s Wet Snow

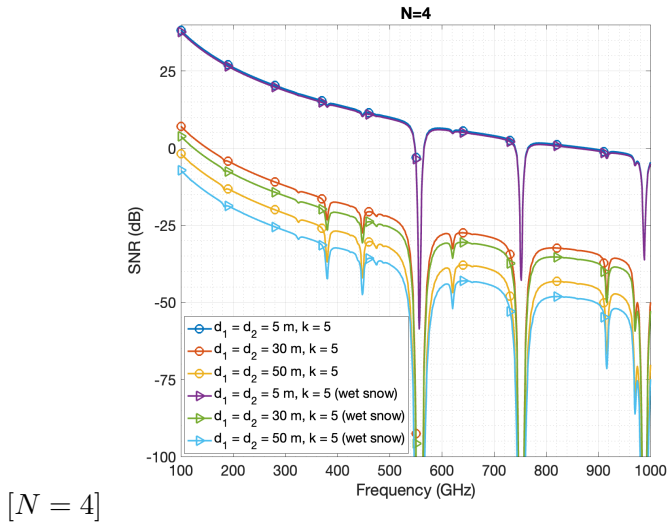

$[N = 4]$

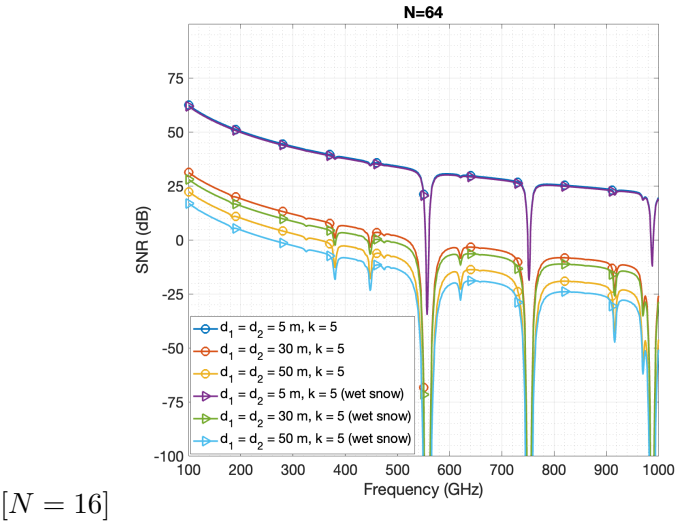

$[N = 16]$

Figure 4.1: Impact of Frequency on the RIS-aided THz-V2VC.

Fig. 4.1 shows the behaviour of SNR against different values of frequenices in a typical RIS-assisted THz-V2V communication system for different values of N ($\in 4, 64$) and d_{SR}($\in 5, 30, 50$)m. As seen in Fig. 4.1, loss in the signal power increases (i.e., SNR decreases) with increasing carrier frequency and distance d_{SR}. As evident from Figs. 4.1(a) and 4.1(b), increasing $N = 4$ to $N = 64$ gives an improvement in the SNR by 20 dB. Further, the impact of wet snow is highlighted in Fig. 4.1. It is clear from the plots that for larger distances, that is, $d_{SR} = d_{RD} = 30$m, the THz signal goes through much more attenuation and consequently the SNR decreases. It could be observed that N and d_{SR} has a very crucial role to play in order to determine the performance of the proposed system.

4.2 SNR v/s d_{SR} and K: THz-V2V v/s V-VLC

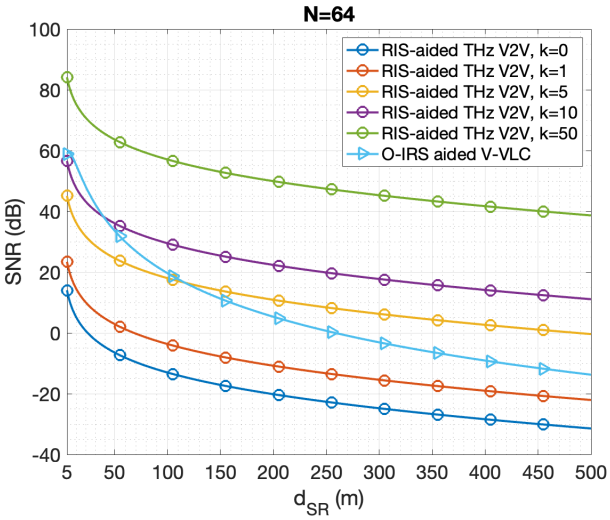

$[N = 64]$

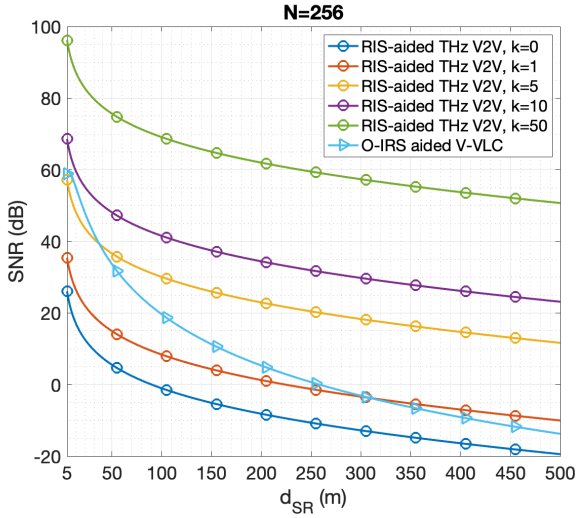

$[N = 256]$

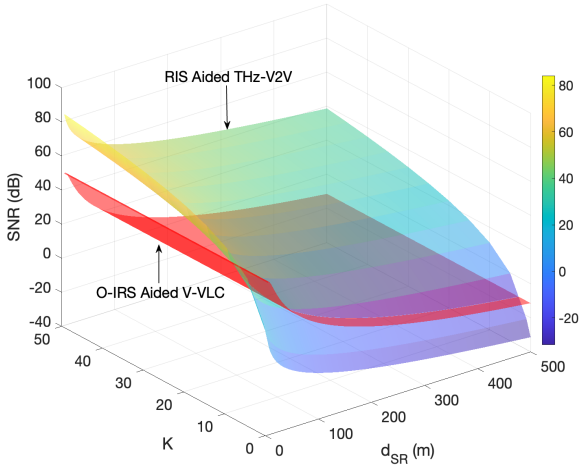

[SNR v/s K v/s d_{SR}, $N = 256$]

Figure 4.2: Impact of d_{SR} and K on the RIS-aided THz-V2VC, $d_{RD} = 10$m, $f = 400GHz$.

Now, we present the impact of d_{SR} and the Rician factor, K on the SNR. We also provide comparative results between RIS-aided THz V2V and O-IRS aided V-VLC systems for $N = 64$ and $N = 256$, as highlighted in Fig. 4.2. Since channel fading becomes less severe as the Rician factor K increases, we see that the SNR is enhanced substantially. However, the performance of RIS aided THz-V2V is largely dependent on K. For $N = 64$, O-IRS aided V-VLC outperforms the THz-V2V systems with $K = 0, 1$. For a distance up to $d_{SR} = 50$m and $d_{SR} = 110$m, the SNR for V-VLC is more than that of THz with $K = 10$ and $K = 50$ respectively. However, irrespective of N and d_{SR}, $K = 50$ RIS aided THz-V2V always performs significantly better than O-IRS aided V-VLC system. This is also depicted in the 3D plot where SNR is plotted against both K and d_{SR}. For higher values of K, THz-V2V gives higher SNR against V-VLC. Lastly, it is clear from Fig. 4.2(a) and 4.2(b) that the performance of THz-V2V against V-VLC depends on N. To elaborate, for $N = 256$, THz system performs better than V-VLC even for $K = 10$. Whereas, THz with $N = 64, K = 10$ experiences lower values of SNR as compared to V-VLC till $d_{SR} = 50$m.

4.3 sumrate v/s Transmit Power and d_{SR}

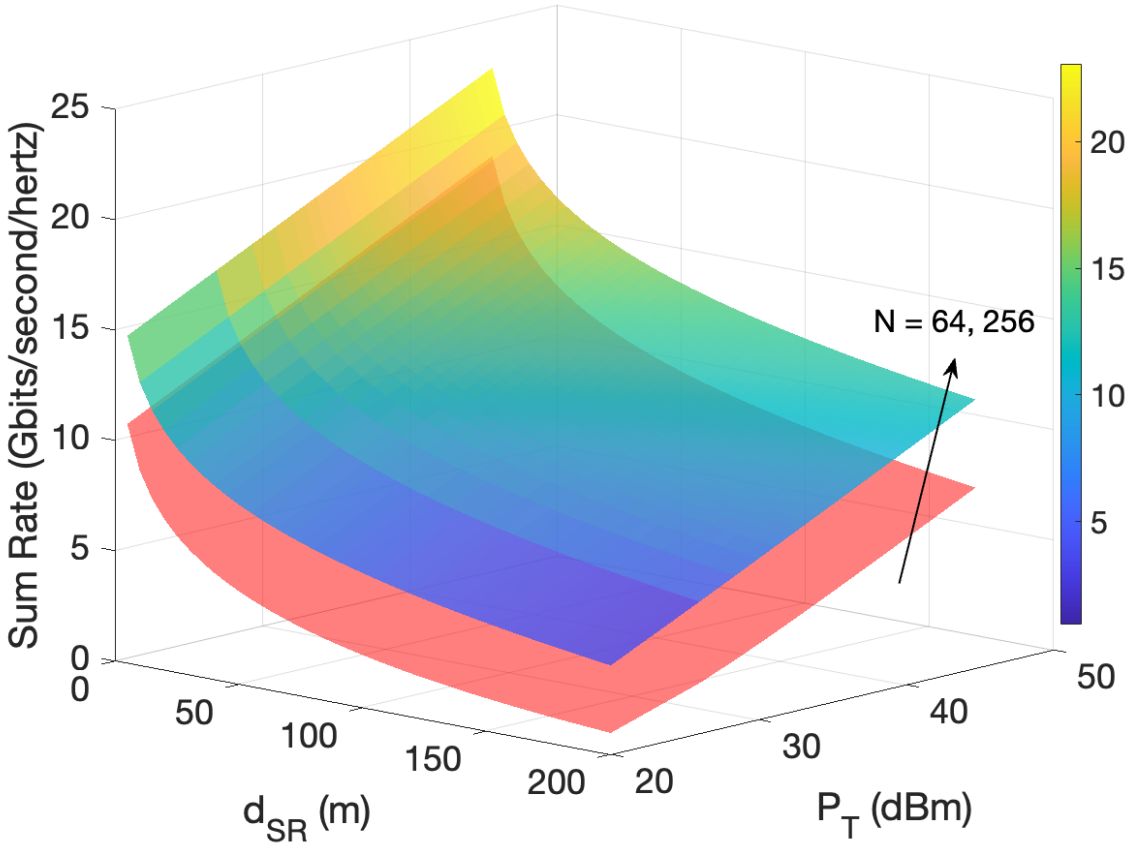

Figure 4.3: Impact of d_{SR} and P_T on Sum Rate.

The sumrate performance of RIS-aided THz-V2V is shown in Fig. 4.3. We plot sumrate $\mathcal{R}$ against d_{SR} and transmit power P_T. We can see that the system performs at its best for $N = 256$. With an increase in P_t, the sumrates produced increases linearly. Results confirm that more transmit power can greatly improve the propagation channel condition.

4.4 BER v/s N: RIS-aided THz-V2V v/s O-IRS-aided V-VLC

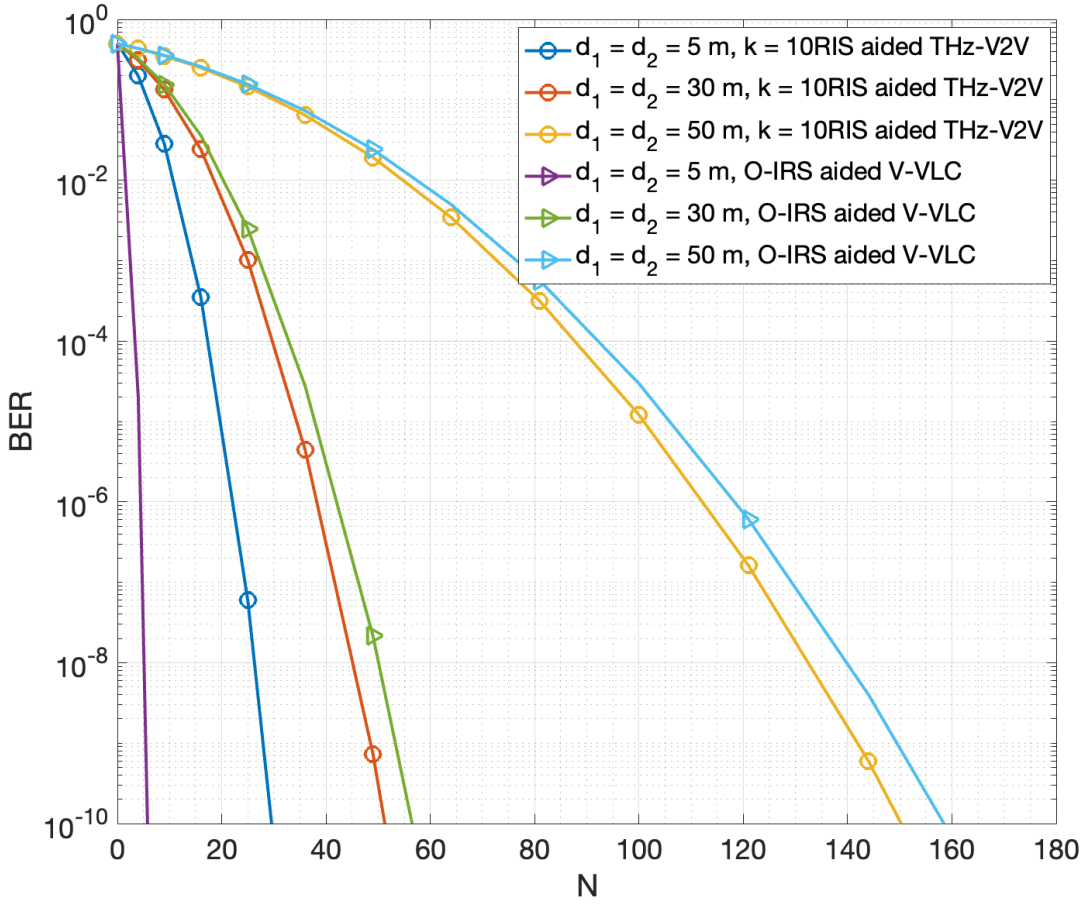

Figure 4.4: Impact of N on BER.

The effect of the number reflecting elements N at the RIS on BER is depicted in Fig. 4.4. Due to stronger received signals, BER performance improves drastically as N increases. It is clear that as d_{SR} increases, there is a degradation of the system efficiency, that is, BER increases. For $d_{SR} = d_{RD} = 30, 50$m, RIS aided THz-V2V gives a better BER when compared to the O-IRS aided V-VLC. However, due to the short communication nature of V-VLC, O-IRS aided V-VLC outperforms the THz-V2V system for $d_{SR} = d_{RD} = 5$m. Hence, distance of source and destination vehicles play a crucial role in determining the quality of such systems.

4.5 BER v/s Transmit Power: THz-V2V under normal weather conditions v/s dry snow conditions

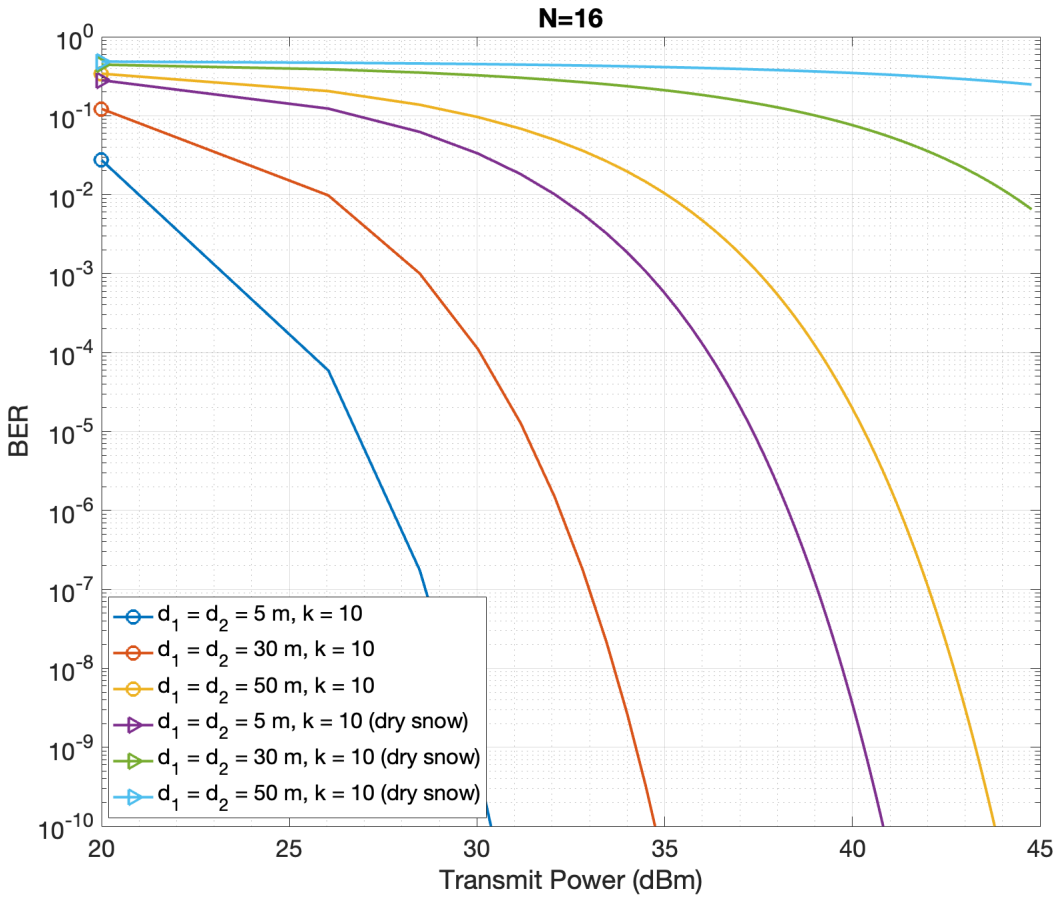

Figure 4.5: Impact of Transmit Power on BER.

Fig. 4.5 highlights the transmit power requirement of the system to achieve a certain BER threshold level under normal and snowy weather condition. As intuitive, with the increase in transmit power, P_T, the BER performance of the system improves. Considering 1×10^{-3} to be the BER threshold for the system, for $d_{SR} = d_{RD} = 5$m, $K = 10$, it requires 22.5 dBm to achieve the required BER. But, under dry snow conditions with the snowfall rate of 10 mm/h, same system would require 34 dBm, that is, 11.5 dB more! Similarly, for $d_{SR} = d_{RD} = 30$m, it requires around 18 dB more to achieve a BER of 0.001 under dry snow atmospheric condition. Hence, while designing such systems, the atmospheric conditions should be taken into account to avoid any communication failures during the mission-critical applications.

Chapter 5

Conclusion

In order to counteract significant propagation loss in THz frequencies, an RIS-assisted THz-V2V system is proposed and analysed in this study. The numerical findings above demonstrate that under certain circumstances, the proposed system performs much better in terms of SNR and sumrate performance than the O-IRS aided V-VLC. Enhanced sumrate performance is obtained in the proposed THz-V2V system if the RIS is placed close to the source or destination vehicle. Furthermore, we also analyze the impact of different atmospheric conditions such as dry and wet snow, rain, etc. to examine the amount of attenuation experienced by the THz-V2V system. Lastly, we study the impact of the number of RIS elements and dry snow weather condition on the BER performance of the proposed system.

Bibliography

[1] H. Elayan, O. Amin, R. M. Shubair, and M.-S. Alouini, "Terahertz communication: The opportunities of wireless technology beyond 5g," in *2018 International Conference on Advanced Communication Technologies and Networking (CommNet)*, 2018, pp. 1–5.

[2] K. Chelli and T. Herfet, "Doppler shift compensation in vehicular communication systems," in *2016 2nd IEEE International Conference on Computer and Communications (ICCC)*, 2016, pp. 2188–2192.

[3] Z. Liu, H. Lee, M. O. Khyam, J. He, D. Pesch, K. Moessner, W. Saad, H. V. Poor *et al.*, "6G for vehicle-to-everything (V2X) communications: Enabling technologies, challenges, and opportunities," *arXiv preprint arXiv:2012.07753*, 2020.

[4] I. F. Akyildiz, C. Han, and S. Nie, "Combating the distance problem in the millimeter wave and terahertz frequency bands," *IEEE Communications Magazine*, vol. 56, no. 6, pp. 102–108, 2018.

[5] M. Shehata, K. Wang, J. Webber, M. Fujita, T. Nagatsuma, and W. Withayachumnankul, "Ieee 802.15.3d-compliant waveforms for terahertz wireless communications," *Journal of Lightwave Technology*, vol. 39, no. 24, pp. 7748–7760, 2021.

[6] Z. Chen, B. Ning, C. Han, Z. Tian, and S. Li, "Intelligent reflecting surface assisted terahertz communications toward 6g," *IEEE Wireless Communications*, vol. 28, no. 6, pp. 110–117, 2021.

[7] S. Hu, F. Rusek, and O. Edfors, "Beyond massive mimo: The potential of data transmission with large intelligent surfaces," *IEEE Transactions on Signal Processing*, vol. 66, no. 10, pp. 2746–2758, 2018.

[8] A. Moldovan, M. A. Ruder, I. F. Akyildiz, and W. H. Gerstacker, "Los and nlos channel modeling for terahertz wireless communication with scattered rays," in *2014 IEEE Globecom Workshops (GC Wkshps)*, 2014, pp. 388–392.

[9] R. B. B. Ke Su, Lothar Moeller and J. F. Federici, "Experimental comparison of terahertz and infrared data signal attenuation in dust clouds," in *J. Opt. Soc. Am. A 29, 2360-2366 (2012)*, 2012, pp. 2360–2366.

[10] P. Siegel, "Terahertz technology in biology and medicine," in *2004 IEEE MTT-S International Microwave Symposium Digest (IEEE Cat. No.04CH37535)*, vol. 3, 2004, pp. 1575–1578 Vol.3.

[11] T. Pal, G. Singh, V. A. Bohara, and A. Srivastava, "Optical IRS Aided B5G V2V Solution for Road Safety Applications," 2022. [Online]. Available: https://arxiv.org/abs/2211.10611

[12] G. Singh, A. Srivastava, and V. A. Bohara, "Impact of weather conditions and interference on the performance of vlc based v2v communication," in *2019 21st International Conference on Transparent Optical Networks (ICTON)*, 2019, pp. 1–4.

[13] S. Priebe, M. Kannicht, M. Jacob, and T. Kürner, "Ultra broadband indoor channel measurements and calibrated ray tracing propagation modeling at thz frequencies," *Journal of Communications and Networks*, vol. 15, no. 6, pp. 547–558, 2013.

[14] J. M. Jornet and I. F. Akyildiz, "Channel modeling and capacity analysis for electromagnetic wireless nanonetworks in the terahertz band," *IEEE Transactions on Wireless Communications*, vol. 10, no. 10, pp. 3211–3221, 2011.

[15] E. Basar, M. Di Renzo, J. De Rosny, M. Debbah, M.-S. Alouini, and R. Zhang, "Wireless communications through reconfigurable intelligent surfaces," *IEEE Access*, vol. 7, pp. 116 753–116 773, 2019.

[16] Proakis, *Digital Communications, 5th Edition New York, NY, USA*. McGraw Hill, 2008.

[17] M. Simon and M. S. Alouini, *Digital Communications Over Fading Channels, 2nd ed. Hoboken, NJ, USA*. Wiley, 2005.

[18] H. R. Pruppacher and J. D. Klett, *Microphysics of clouds and precipitation.* Dordrecht: Kluwer Academic Publishers, 1997.

[19] D. Deirmendjian, *Electromagnetic scattering on spherical polydispersions.* New York: American Elsevier Publishing, 1969.